Max-Planck-Institut
für Meteorologie

REPORT No. 106

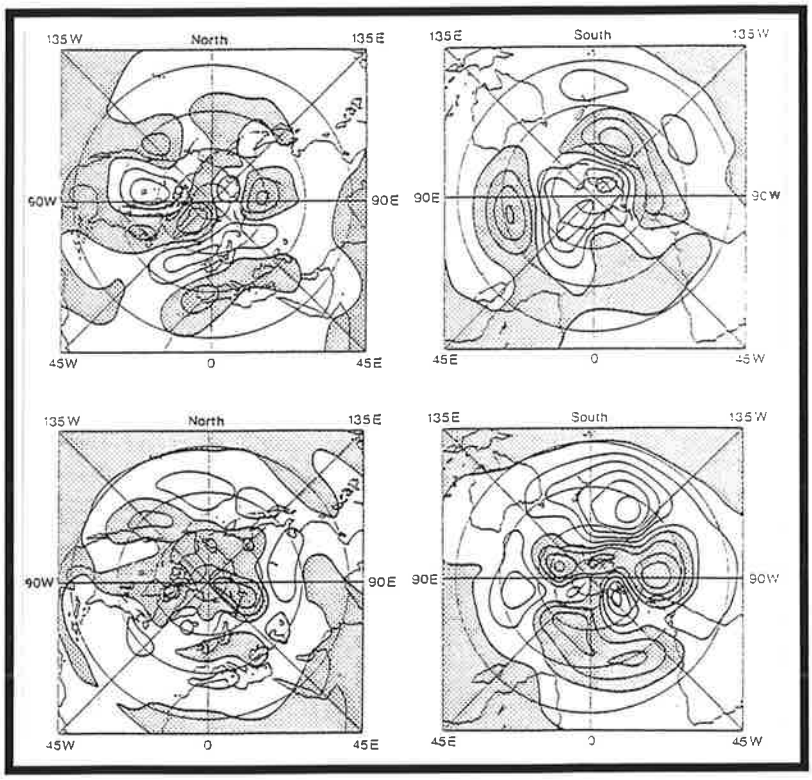

NUMERICAL EXPERIMENTS ON THE ATMOSPHERIC RESPONSE TO COLD EQUATORIAL PACIFIC CONDITIONS ("LA NINA") DURING NORTHERN SUMMER

by

HANS VON STORCH • DIERK SCHRIEVER • KLAUS ARPE
GRANT W. BRANSTATOR • ROBERTO LEGNANI • UWE ULBRICH

HAMBURG, MAY 1993

AUTHORS:

Hans von Storch
Dierk Schriever
Klaus Arpe

Max-Planck-Institut für Meteorologie
Hamburg, Germany

Grant W. Branstator

National Center for Atmospheric Research
Boulder, USA

Roberto Legnani

Instituto per lo Studio delle Metodologie
Geofisiche Ambientali
Modena, Italy

Uwe Ulbrich

Institut für Geophysik und Meteorologie
Köln, Germany

MAX-PLANCK-INSTITUT
FÜR METEOROLOGIE
BUNDESSTRASSE 55
D-2000 HAMBURG 13

Tel.: +49 (040) 411 73 - 0
Telex: 211092mpime d
Telemail: MPI.METEOROLOGY
Telefax: +49 (040) 411 73 - 298

Numerical Experiments on the Atmospheric Response to Cold Equatorial Pacific Conditions ("La Nina") During Northern Summer

Hans von Storch, Dierk Schriever and Klaus Arpe
Max-Planck-Institut für Meteorologie, Hamburg, Germany

Grant W. Branstator
National Center for Atmospheric Research, Boulder, USA

Roberto Legnani
Instituto per lo Studio delle Metodologie Geofisiche Ambientali, Modena, Italy

Uwe Ulbrich
Institut für Geophysik und Meteorologie, Köln, Germany

ISSN 0937 – 1060

Abstract

The effect of cold conditions in the central and eastern Equatorial Pacific during Northern Summer is examined in a series of numerical experiments with the low resolution (T21) atmospheric general circulation model ECHAM2. Anomalous sea surface temperatures (SST) as observed in June 1988 were prescribed and the effect on the global circulation is examined.

In the model atmosphere, the anomalous cold water in the Equatorial Pacific excites a strong and stable response over the tropical Central and East Pacific. From here stationary Rossby waves radiate into both hemispheres. The Northern Hemisphere wave train is weak and affects only the Northeast Pacific area; the Southern Hemisphere wave train arches from the Central Pacific over the southern tip of South America to the South Atlantic. This response is not only present in the basic anomaly experiment with the T21 GCM but also in experiments with SST anomalies confined to the tropics and with an envelope-formulation of the SST anomalies, in experiments with a linear model, and in high resolution (T42) model experiments.

The model output is also compared to the actually observed atmospheric state in June 1988. The model simulations do not reproduce the global circulation anomalies which were observed in June 1988. The model experiments are inconclusive with respect to the question of whether the North American drought observed in summer 1988 was related to the anomalous SST conditions in the Subtropical and Tropical Pacific. An explanatory analysis with a linear model reacting to prescribed heating anomalies as well as with the high-resolution GCM indicates that the model overreacted to the equatorial SST anomalies but almost ignored the contemporaneous subtropical SST anomalies on the Southern Hemisphere.

1. INTRODUCTION

Numerous numerical experiments with General Circulation Models (GCMs) have been performed on the effect that an "El Niño" or an "La Niña" event may have on the thermodynamic and hydrodynamic state of the atmosphere (e.g., Blackmon et al., 1983, Cubasch, 1985). Most of these experiments were done as paired sensitivity experiments. One run was integrated with standard sea surface temperature (SST) and another was integrated with an idealized or observed sea-surface temperature (SST) anomaly added to the climatological SST distribution. Most of the experiments were done with warm conditions (El Niño); less effort has been put into the analysis of cold conditions (La Niña). All experiments have been concerned with the effect of such anomalies on an atmosphere during Northern Hemisphere winter. The typical result has been that the northern winter SST anomalies in the Equatorial Pacific yield a marked modification of the tropical Hadley and Walker Cells, tropical heating anomalies from which wave trains radiate into the Northern Hemisphere, and no significant response in the (summer) Southern Hemisphere. Trenberth and Branstator (1988), Lau and Peng (1992), Mo et al. (1991) and Karoly (1989) have suggested that tropical SST anomalies may also be important to midlatitudes during northern summer. To test this hypothesis we have performed a series of numerical experiments with the ECHAM GCM and examined the atmospheric response to specified SST anomalies when the mean state represents southern winter.

To have the possibility to compare the numerical results with observed data we use an observed SST anomaly field to force the atmospheric GCM. Since very strong negative SST anomalies (maximum anomalies were larger than -3K; Fig. 1) prevailed in June 1988 in the Equatorial Pacific we have chosen the SST anomalies of June 1988. That the June 1988 anomalies were extraordinary is shown by the "homogenized" SST-SO index (Wright, 1984, 89) in June from 1870 to 1990 (Fig. 2). Wright's index, which is an average of SST over part of the eastern equatorial Pacific, is very similar to the operational "Niño 3"-index compiled by the US Climate Analysis Center. The June 1988 index of -1.5 K is the second lowest June value in the record. Only in 1916 was an even lower value of -2.1 K constructed from the data (Fig. 2) and this value may be affected by a cold bias prior to 1940 that may be partially the result of an instrumental problem (Folland and Parker, 1990).

By choosing the June 1988 SST distribution to do the sensitivity experiments we hoped to be able to contribute to the discussion on the mechanisms which

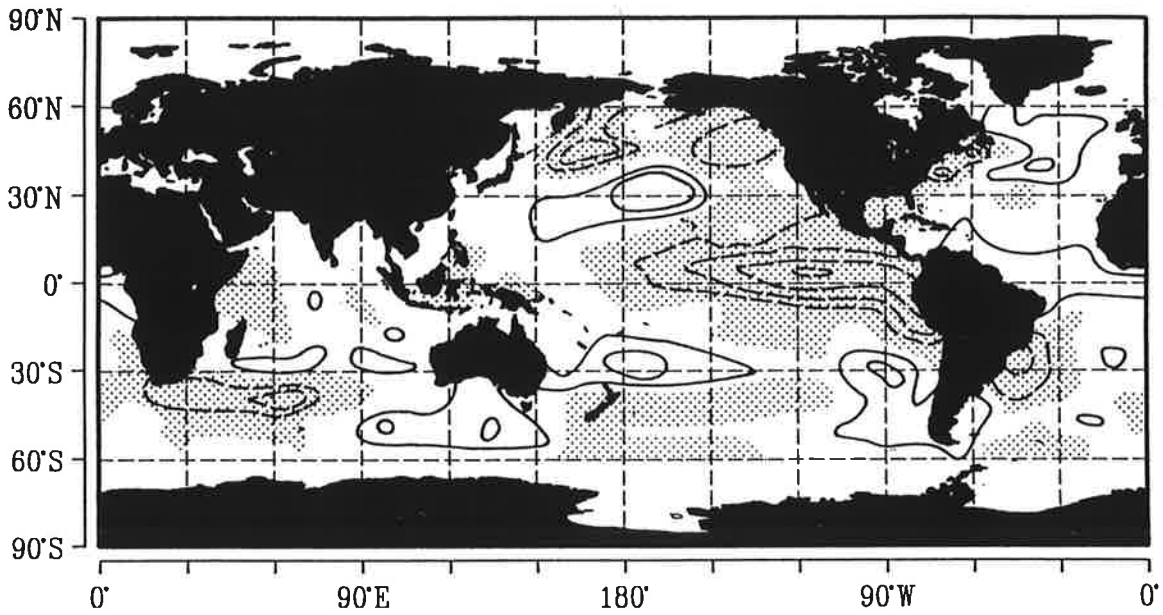

Figure 1:
Sea surface temperature (SST) anomalies in June 1988 as analyzed by the US Climate Analysis Center (CAC) relative to the 1979-1988 mean. The zero line is emboldened, negative values are dashed. Isolines: ± 0.5, 1, 2 and 3 K.
The SST anomaly that was published by CAC (US Department of Commerce, 1988) deviates from our map because we use a different base period, namely 1979 through 1988, to calculate the anomalies. The rational for doing so is that the ECMWF analyses are available for that period and that the additional runs discussed in Section 5 were done with this climatology.

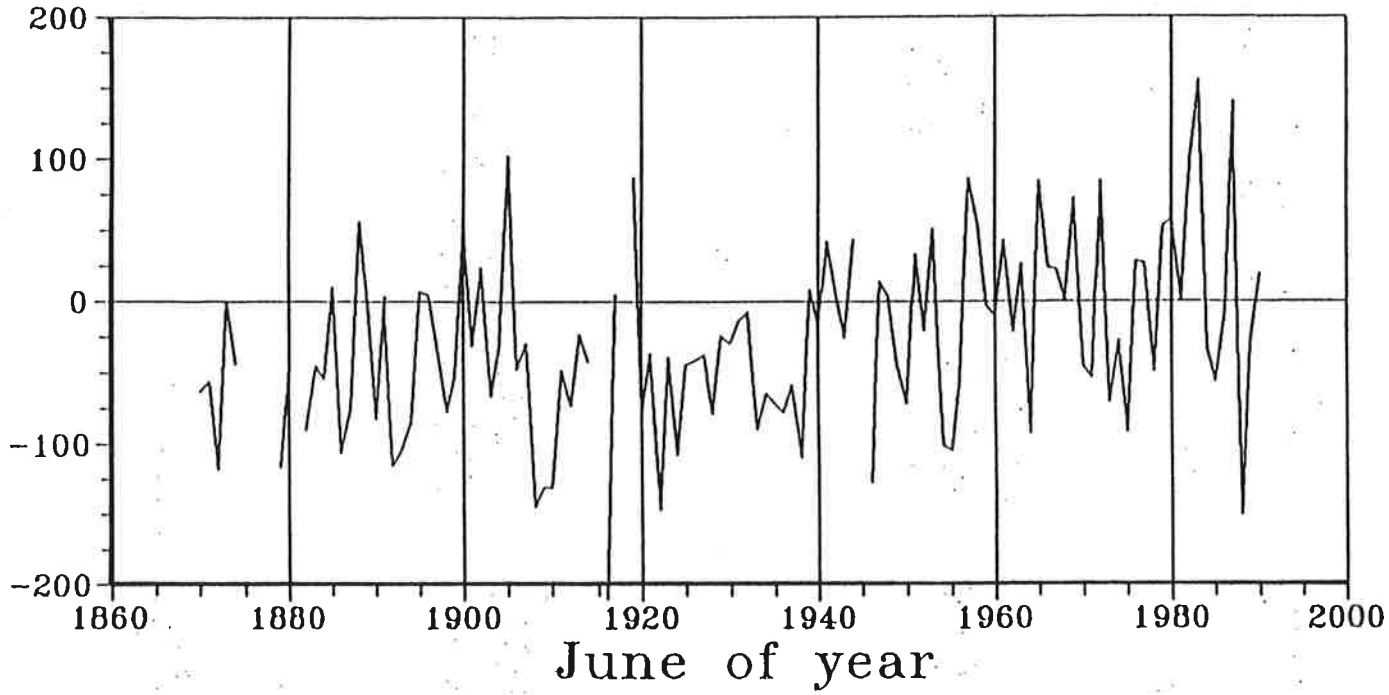

Figure 2:
Wright's (1989) SST index of the Southern Oscillation in June. Units: 10^{-2}K.

lead to the North American drought in summer 1988 (Trenberth et al (1988), Trenberth and Branstator (1992), Palmer and Brankovic (1989), Mo et al. (1991)). However, as will be shown in the present paper our experiments do not help to understand the mechanisms responsible for the formation or maintenance of the US drought, simply because of the failure of the model to reproduce the tropical circulation anomalies observed during June 1988. Nevertheless, as described in our exposition, they are useful for investigating the more general question of the influence of equatorial Pacific heating anomalies on the atmosphere's circulation during northern summer.

The organization of the paper is as follows: In Section 2 we describe the GCM experiments and the diagnostic techniques. In Section 3 the anomalies excited by the anomalous SST distribution, as derived from the paired GCM experiments with and without SST anomalies, are described and compared with observed data. A set of three experiments with SST anomalies that are different from those in the basic experiment is discussed in Section 4: In one experiment a pool of extra warm water north of the East Pacific ITCZ is introduced; in the second experiment the SST anomalies are limited to the tropics equatorward of 30° latitude and in the third experiment an "envelope" formulation is used for the SST anomalies. The paper concludes with a discussion of the results, including a comparison with results obtained by the same GCM integrated with seasonally changing boundary conditions in high (T42) resolution. Also, we discuss our results in the framework of linear theory in the closing Section 5.

2. GCM EXPERIMENTS AND DIAGNOSTIC TOOLS

We have made a series of five GCM experiments with the ECHAM2-model in T21 horizontal resolution (Roeckner, et al., 1989). This model has been used successfully in GCM sensitivity studies (e.g., Ulbrich et al., 1993, Weber et al., 1993) as well as in climate change experiments (Cubasch et al., 1992). To save computer time and to obtain a maximum number of statistically independent realizations, the GCM runs were done in the permanent June mode. Each run was extended over 24 months. The first month of each run was regarded as a spin-up period and discarded.

The first of these five experiments was the "control" run, which was made with the climatological (defined as 1979-1988 average) SST projected on the $5.6^{\circ}\times5.6^{\circ}$ Gaussian grid. In the second, referred to as "standard" SST anomaly run (SSTA), the June 1988 SST anomaly projected on the $5.6^{\circ}\times5.6^{\circ}$ Gaussian grid (Fig. 4) was super-imposed on the climatological SST. The control and the standard anomaly run are compared in Section 3. The remaining three runs with this model were sensitivity experiments, each with a different SST distribution (Section 4).

In addition of the ECHAM2 experiments, two realizations for the June-1988 atmospheric circulation anomalies were available from two statistically independent 10-year runs with a different version (namely ECHAM3) of the same GCM but with doubled horizontal resolution (i.e., T42). These are discussed in Section 5.

One means we have used to analyze the experiments is the univariate recurrence analysis (von Storch and Zwiers, 1988). This technique is a tool to measure the statistical stability of the GCM response. An anomaly random variable $\mathbf{X}$ is said to be (at least) p-recurrent compared to a control random variable $\mathbf{Y}$ if

$$(*) \qquad \mathbf{P}(X > \bar{\mathbf{Y}}) > p$$

where $\mathbf{P}(\cdot)$ is the probability that the statement in the parentheses is true. X is a randomly selected realization of the anomaly variable $\mathbf{X}$ and $\bar{\mathbf{Y}}$ the mean of the control ensemble $\mathbf{Y}$. In our applications, the random variables $\mathbf{X}$ and $\mathbf{Y}$ are monthly means of, for example, velocity potential at 200 hPa in two runs that are compared (e.g., SSTA run vs. control run). If the two random variables $\mathbf{X}$ and $\mathbf{Y}$ are Gaussian and share the same standard deviation σ, the maximum p fulfilling (*) is

(**) $$p = S^{1}\left[\frac{\bar{X} - \bar{Y}}{\sigma} \right]$$

if $\bar{X} > \bar{Y}$ (von Storch and Zwiers, 1988). S is the cumulative distribution function of the Gaussian distribution. In the following sections maps of the univariately estimated level p of recurrence are shown. A discussion of the relationship between the recurrence analysis and the conventional t-test is in the Appendix.

We compare our results against observations of out-going long-wave radiation, monitored by the US National Meteorological Center, and against analyses prepared by the European Centre for Medium Range Forecasts (ECMWF). For different parameters we use different years to define the climatology that is used to compute the anomalies. For geopotential height at 500 hPa the mean of the years 1979, 1981-88 serves as climatology. The choice of these years is consistent with the choice of the SST climatology, namely 1979 through 1988, which is used in the control run. The 1980 data were not available due to local logistical problems. For the velocity potential as well as for the stream function we use a different base period, namely 1983 through 1991, because of analysis weaknesses with respect to the tropics and the divergent flow, in the early years of the operational ECMWF analysis.

3. THE BASIC EXPERIMENT: STANDARD SST ANOMALY RUN VERSUS CONTROL RUN

In this section we compare the two T21-GCM runs which were integrated with climatological SST (1979 - 1988 average) and with the global June 1988 SST anomaly (Fig. 1) superimposed. In Subsection 3.1 height-latitude cross sections of a number of zonally averaged parameters derived from the control run and from the experimental run are compared in order to give an impression of the latitude-height distribution of the signals. In Subsection 3.2 we consider single level horizontal distributions of 200 hPa velocity potential and stream function, hemispheric distributions of 500 hPa height and tropical OLR (out-going long-wave radiation), and we compare these parameters against observations.

3.1 Zonally averaged quantities

The SST experiment minus control difference fields of a number of zonally averaged parameters are plotted in Figure 3. The parameters vertical "velocity" (Fig. 3a), zonal wind (Fig. 3b), temperature (Fig. 3c) and specific humidity {Fig. 3d) have been chosen for allowing for an overall impression of the hydro- and thermodynamics of the response to the anomalous SST. The local level of recurrence is indicated by stippling - light stippling refers to $p \geq 80\%$ or $p \leq 20\%$ and heavy stippling to $p \geq 95\%$ or $p \leq 5\%$.

The tropical wind field, as given by the vertical velocity in pressure coordinates ω (Figs. 3a) and by the zonal wind u (Fig. 3b), is markedly perturbed by the anomalous SST with a statistical stability of $p \leq 20\%$ or $p \geq 80\%$ in many areas equatorward of 30^0 latitude. The enhancement of the low level equatorial easterlies by up to -0.5 m/s is statistically very stable ($p \leq 5\%$). In the upper troposphere there are anomalous easterlies in the subtropics and anomalous westerlies along the equator. The Hadley Cell, as given by the vertical "velocity" ω, is weakened with anomalous downward movement at the equator (maximum ≥ 6 mPa/s) and anomalous upward movement in the descending branches of the Hadley Cell (minimum ≤ -4 mPa/s). All these features are similar to anomalies associated with warm events but with opposite polarity. In the Northern Hemisphere the Ferrel Cell seems to be modified also, but the statistical stability of this effect is only moderate.

The statistically stable response of the temperature field and of the specific humidity field (Figs. 3c and d) is mostly confined to the equatorial

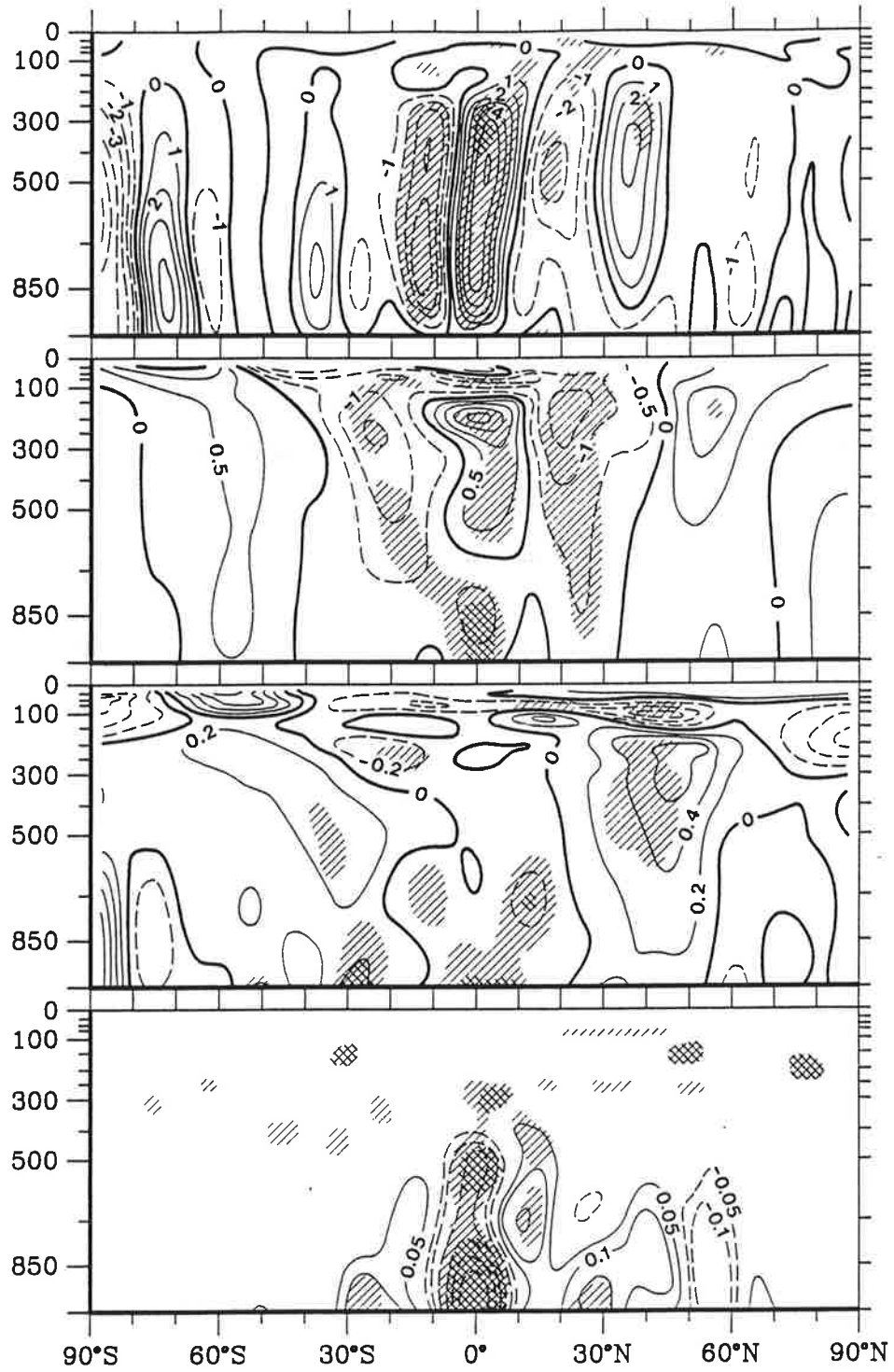

Figure 3

Latitude-height cross section of "SST-experiment minus control" difference fields for a number of zonally averaged parameters. The local level of recurrence p is given by the stippling. Light stippling represents $p \geq 80\%$ or $p \leq 20\%$, and heavy stippling $p \leq 5\%$ or $p \geq 95\%$.

a) Vertical velocity in pressure coordinates ω (spacing: 1 mPa/s)

b) Zonal component u of the wind (spacing: 0.5 m/s)

c) Temperature (spacing: 1 K)

d) Specific humidity (spacing 0.1 g/kg)

troposphere. The reduction of specific humidity below 700 hPa, with largest anomalies of approximately 0.5 g/kg, is very stable with $p < 5\%$. Maximum tropical temperature anomalies of -0.2 K are also mostly below 700 hPa. This can be readily understood, as reduced sea-surface temperatures lead to reduced evaporation with the effect of less moisture in the ascending air. Subsequently less latent energy is released so that the Hadley circulation is weakened. In the upper troposphere at about 40°N there is a warming, of up to 0.6 K with $p \geq 80\%$, which likely is due sinking (Fig. 3a).

3.2 The response in terms of horizontal distributions

The model responds to the SST anomaly with a marked change of its divergent flow, as expressed by the velocity potential anomaly at 200 hPa (Fig. 4b). An anomalous divergent tropical zonally oriented cell connects the Indian Ocean and the Eastern Pacific, with maximum westerly divergent wind anomalies at 200 hPa over the Maritime Continent while anomalies easterlies flow across South America. The induced anomalies vary between $-3 \cdot 10^{-6} m^2 s^{-1}$ and $6 \cdot 10^{-6} m^2 s^{-1}$, and are highly recurrent, especially over the North Pacific (Fig. 4a).

In Fig. 4c, the anomalous 200 hPa velocity potential field of June 88, as derived from ECMWF analyses, is given. The similarity with the simulated field (Fig. 4b) is moderate. In the analyses there are two anomalous upper air convergent zones, over the Maritime Continent and over the East Pacific, and two anomalous divergent areas, over the Tropical Atlantic and over the Western Indian Ocean. The two divergent areas are reproduced by the model, but the two convergent areas are merged together and placed in the Central Pacific.

In the model there is also a statistically stable signal in rotational flow (Fig. 5). An anomalous 200 hPa stream function dipole straddles the equator in the Central / Western Pacific with upper level westerly wind and recurrence levels $p \leq 1\%$ and $p \geq 99\%$. A weaker equatorial dipole of opposite polarity occurs over South America. From the eastern Pacific a wave train appears to radiate to North America. Over North America the stream function surface is anomalously high ($p \geq 80\%$) but exhibits only weak gradients. Relatively large but only weakly stable anomalies appear in the winter (southern) hemisphere.

The anomalies derived from the ECMWF analyses share little with the simulated fields (Fig. 5c). The most striking difference is the absence of the dipole in the tropical East Pacific. However, in the Atlantic sector there are some

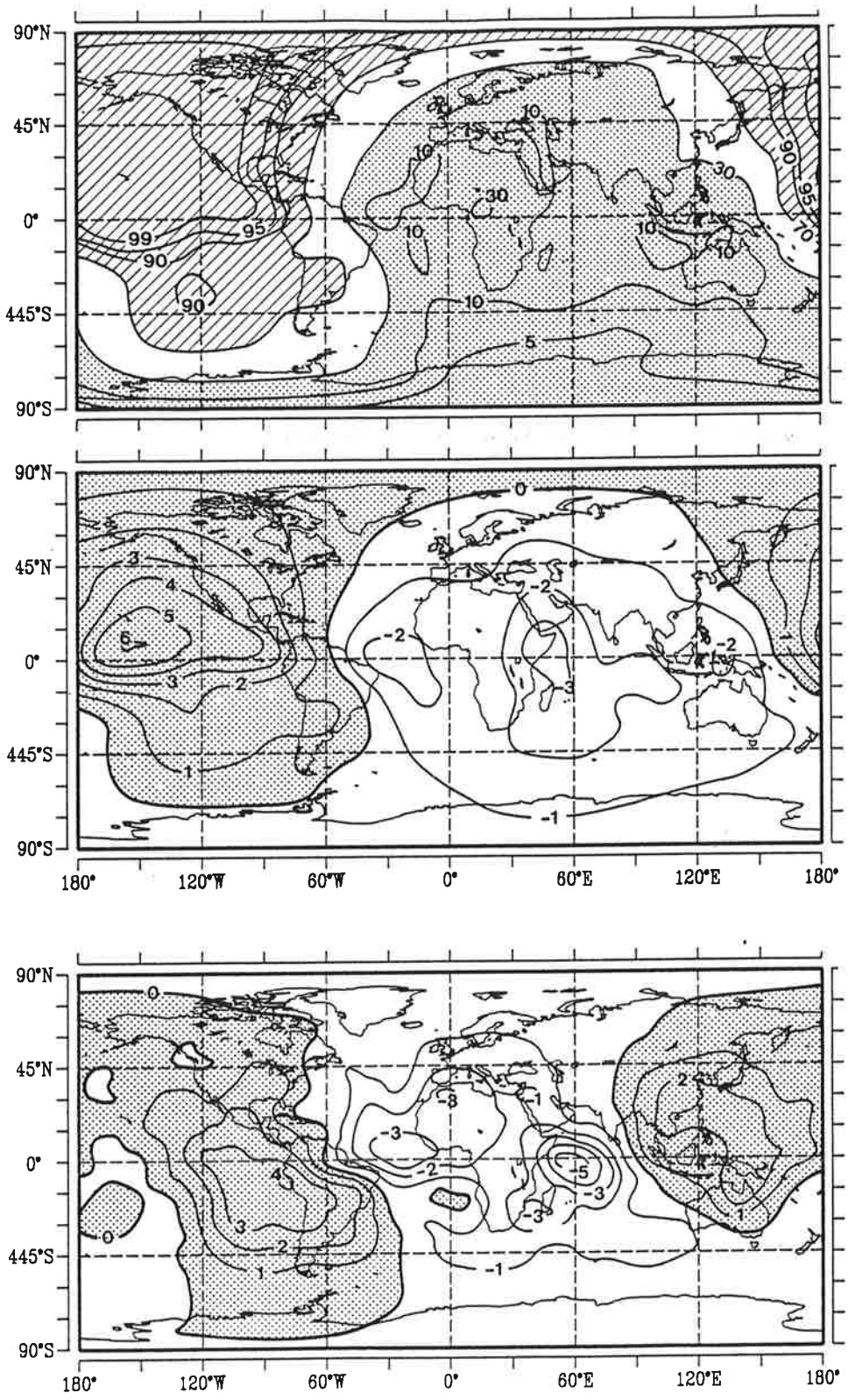

Figure 4

The 200 hPa velocity potential field in the standard SST anomaly run (SSTA) and in the control run.

a) Local level of recurrence. The heavy stippling represents $p \geq 80\%$, the light stippling indicates $p \leq 20\%$.

b) Difference field "SSTA minus control" in 10^6 m^2s^{-1}.

c) Observed anomaly, relative to the 1983-91 mean, in 10^6 m^2s^{-1}.

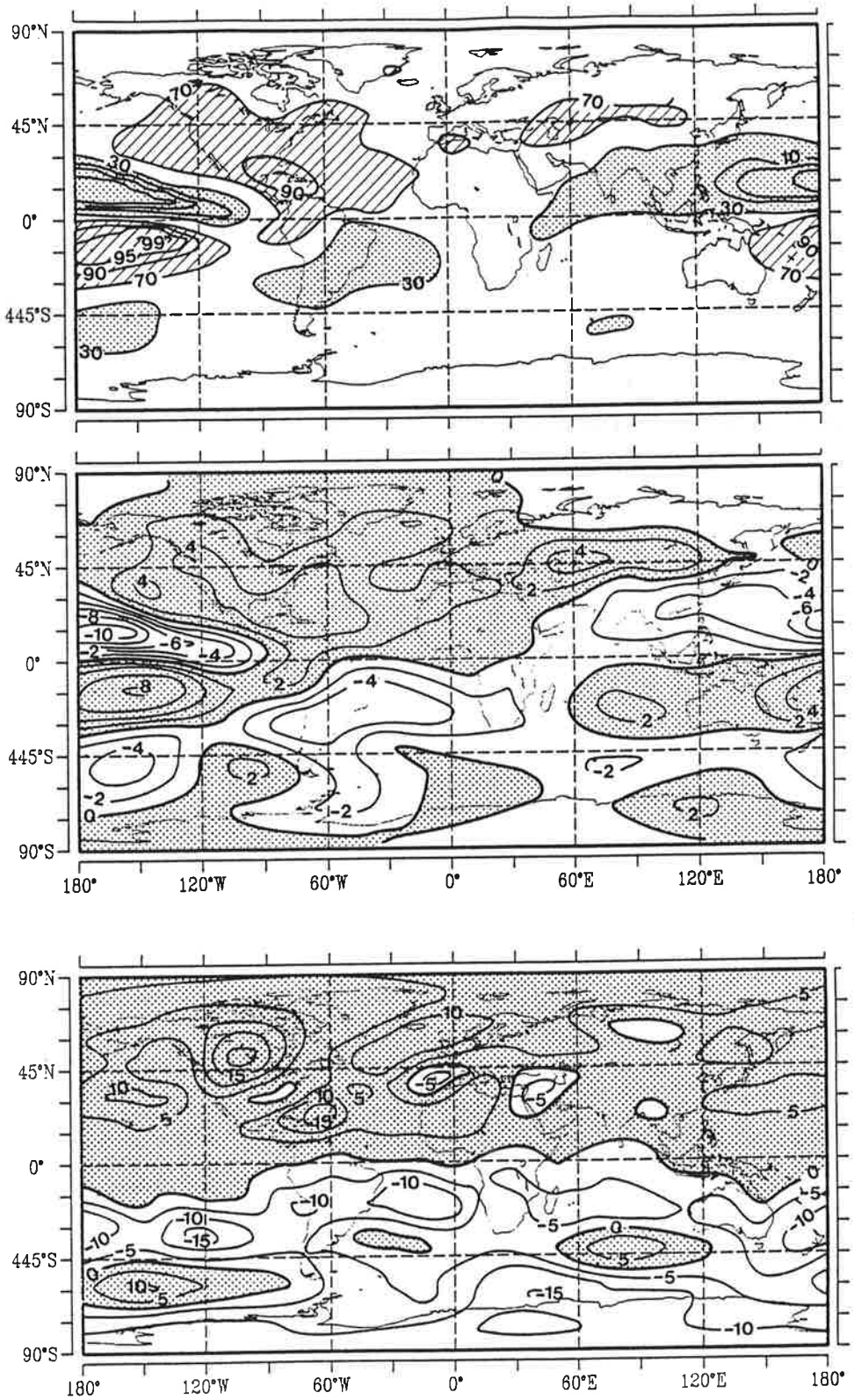

Figure 5

The 200 hPa stream function field in the basic SST anomaly run (SSTA) and in the control run.

a) Local level of recurrence. The heavy stippling represents $p \geq 80\%$, the light stippling indicates $p \leq 20\%$.

b) Difference field "SSTA minus control" in 10^6 m^2s^{-1}.

c) Observed anomaly, relative to the 1983-91 mean, in 10^6 m^2s^{-1}.

similarities not only in the tropics but also in the extratropics of both hemispheres.

The response in tropical outgoing long-wave radiation (Fig. 6b) has marked positive anomalies (maximum of 60 Wm^{-2}; $p \geq 99\%$) in the Eastern Pacific and weak negative anomalies in most of the remaining tropics. The observed anomalies for June 1988 are shown in Fig. 6a. The patterns of the simulated and observed OLR anomaly are generally consistent over many regions, with negative anomalies less than -15 Wm^{-2} over Northern South America and the Tropical Atlantic, the West Pacific and the South Pacific Convergence Zone (SPCZ), and with positive anomalies greater than 15 Wm^{-2} along the equator in the Eastern Pacific. A major discrepancy occurs in the ITCZ in the Eastern Pacific; here anomalies less than -15 Wm^{-2} were observed but the simulated anomalies are small. It was this area that was identified by Trenberth et al. (1988) and Trenberth and Branstator (1992) as being instrumental in causing the US drought. We come back to this point in Section 4.1. A second discrepancy is the much larger amplitude in the equatorial Eastern Pacific anomaly in the GCM. Note that the comparison of Figs. 6a and 6b is not fully consistent: the climatological means, relative to which the anomalies are defined, are different in the two figures.

Fig. 7 shows for both hemispheres the mean 500 hPa height SSTA minus control difference maps and the anomalous 500 hPa height field as observed in June 1988. In the observation (Fig. 7a) most of the North American continent is covered by an anticyclone with a maximum anomaly of 100 m. This anticyclone is only very weakly present in the model solution (Fig. 7b). In the GCM upstream of the anticyclone a low is placed just off the US west coast and a weak high lies over the Central North Pacific. The high and the low in the North Pacific are reproduced (Fig. 7b) with $p \geq 95\%$ and $p \leq 30\%$ (not shown). There are significant differences in magnitude between the observed anomaly and the simulated anomaly: the model underestimates the observed anomalies by a factor of four and more. Part of this systematic underestimation may be due to the fact that the observed anomaly is calculated from just one month whereas the simulated anomaly represents a 24 months mean.

The observed Southern Hemisphere anomalous height field (Fig. 7c) exhibits an elongated ridge at 30°S from Australia to South America with a maximum of 40 m. It also has a strong low at 60°S in the Indian Ocean and a trough at 60°S extending from 130°E to 80°W. Over Antarctica an anomalous high existed in June 1988. In the simulation (Fig. 7d) there is also an anomalous ridge at

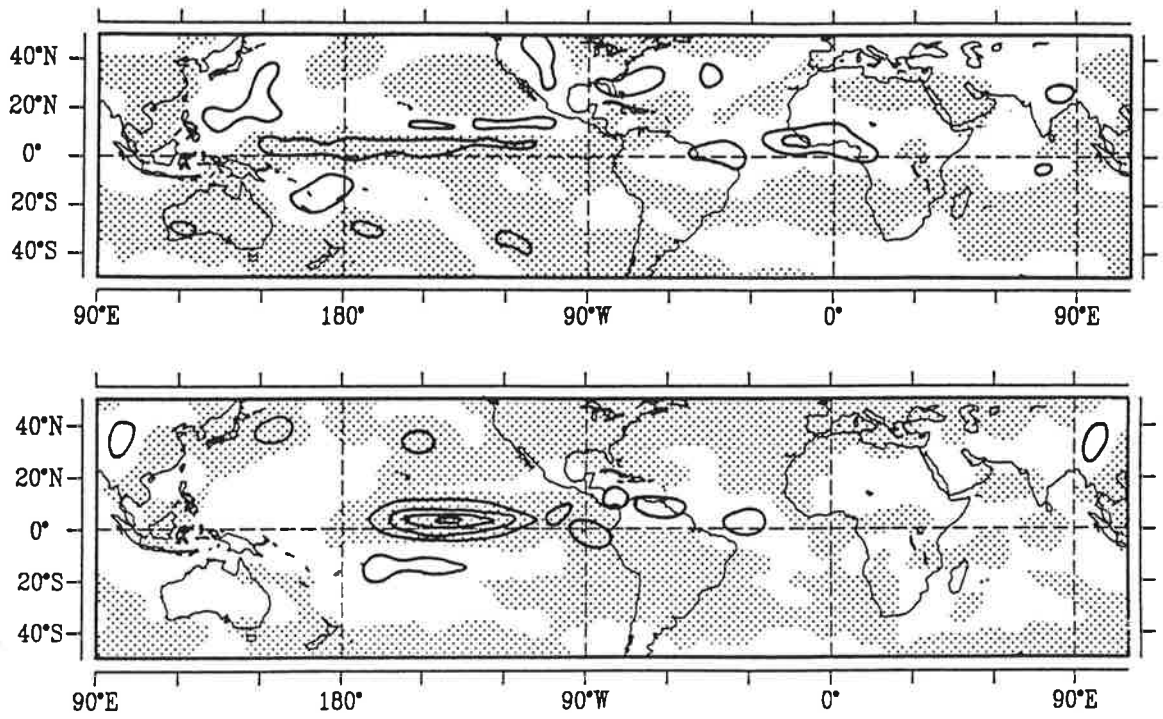

Figure 6

Anomalies of outgoing long-wave radiation (OLR). Positive values, indicating reduced convection and rainfall, are stippled. Spacing: 15 Wm^{-2}.

a) Observed anomaly in June 1988 (US Department of Commerce, 1988)

b) "SSTA minus control" difference field.

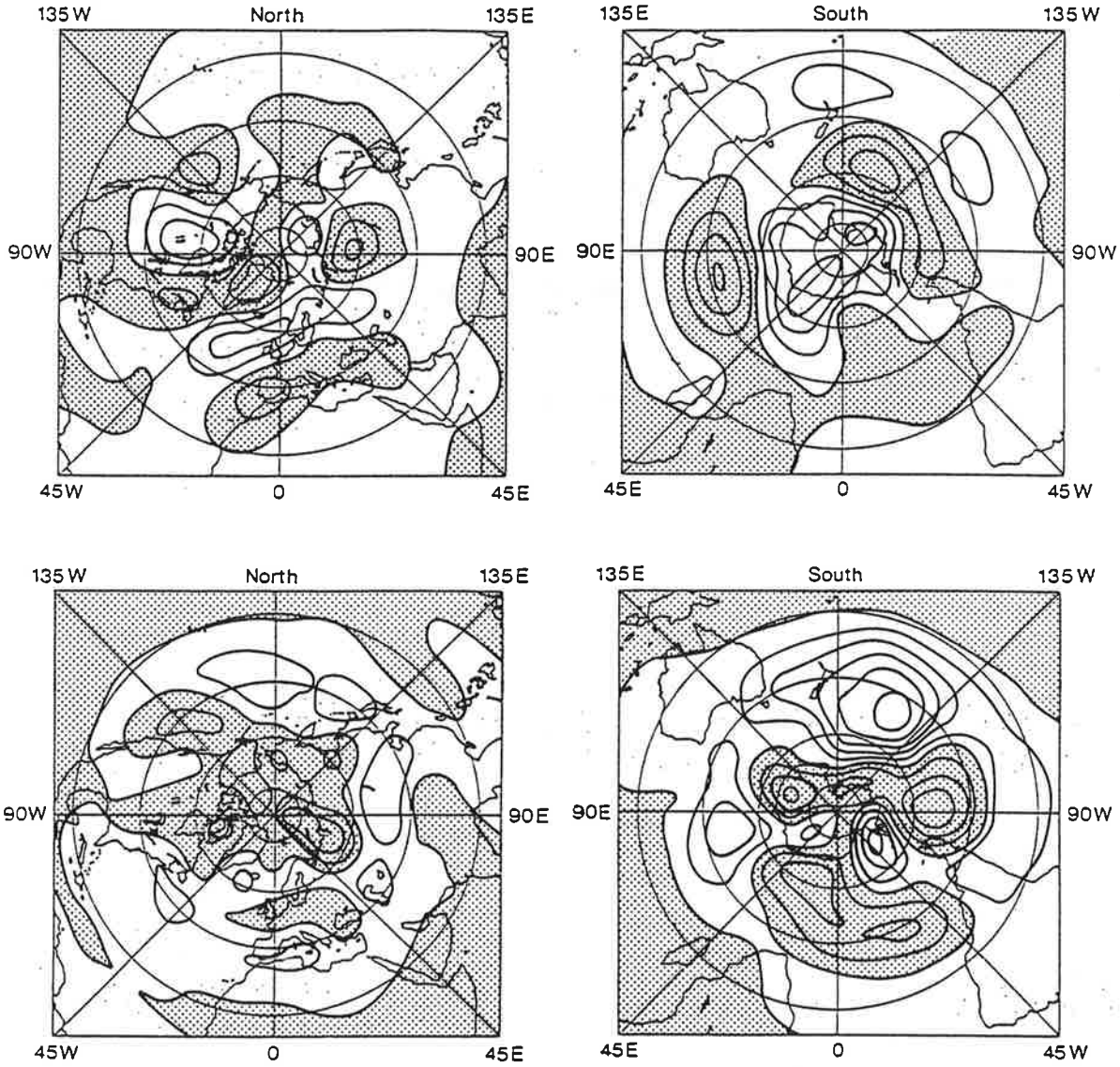

Figure 7

500 hPa height in the SSTA vs. control experiment and in the observations. The observations are derived from ECMWF analyses, and the climatology is defined as the 1979 and 1981 - 88 mean (1980 is disregarded because of logistical problems).

a) Observed anomaly in June 1988 in the Northern Hemisphere. Spacing: 40m.

b) SSTA-control difference field in the Northern Hemisphere. Spacing: 10m.

c) Observed anomaly in June 1988 in the Southern Hemisphere. Spacing: 40m.

d) SSTA-control difference field in the Southern Hemisphere. Spacing: 10m.

30°S from Australia to South America, with $p \geq 70\%$, but this ridge is in the Western Pacific and is much broader than in the observations. In the model the trough at 60°S in the Pacific is limited to the East Pacific ($p \leq 30\%$). In the sector between 135°W and Greenwich the modeled and observed patterns are similar, but in the Indian Ocean and over Antarctica the two patterns are different.

4. ADDITIONAL EXPERIMENTS WITH DIFFERENT SPECIFIED SST ANOMALIES

Three more experiments with different specified SST anomalies were made with the T21 GCM to shed more light on the effect of the anomalous SST distribution. In one experiment an extra pool of warm water north of the equator was introduced in the eastern Pacific (Fig. 8a); in a second experiment the anomalies were limited to the tropical Pacific (Fig. 8b) and in a third experiment an "envelope" formulation was used for the SST (Fig. 8c).

4.1 Warm water pool north of the Pacific ITCZ

The anticyclone that was observed in June 1988 over North America is not well reproduced by the GCM (Fig. 9). One possibility for this failure is that there is no patch of extra warm water at about 10°N in the Eastern Tropical Pacific in our SST anomaly field. Such a pool was identified by Trenberth et al. (1988) and Trenberth and Branstator (1992) as the dominant agent for the forming of the drought. We have lost this pool because we used a different climatology than Trenberth et al.; also the averaging of the SST anomalies on the relatively coarse 5.6°×5.6° T21 grid might have had an effect. To test the "warm pool" hypothesis an additional GCM experiment was done. In the region from the dateline to the American coast and from about 17° to 28°N the SST was enhanced by 3 K whereas everywhere else the standard SST anomaly was used (Fig. 8a).

Our GCM produces a clear OLR-response to the additional warm water (Fig. 9a): Just above the maximum of 3 K, OLR is greatly reduced ($\leq$ -30 Wm^{-2}; $p \leq 1\%$) but elsewhere there is little change. The 500 hPa topography in the Southern Hemisphere (Fig. 10a) is almost the same as in the basic experiment (Fig. 7d), but in the Northern Hemisphere there is a marked change in the Pacific sector (Fig. 10a). A wavetrain with an amplitude larger than in the basic experiment (Fig. 7b) emanates from the tropical or subtropical Pacific. Just as in the basic experiment this wavetrain is shifted to the west of the observed wavetrain and places an anomalous low over central North America.

We conclude from this experiment that the patch of warm water in the eastern part of the subtropical Pacific had the potential to affect the atmospheric circulation over the North Pacific. Our modification of the SST did, however, not yield a response that was more similar to the observed June 1988

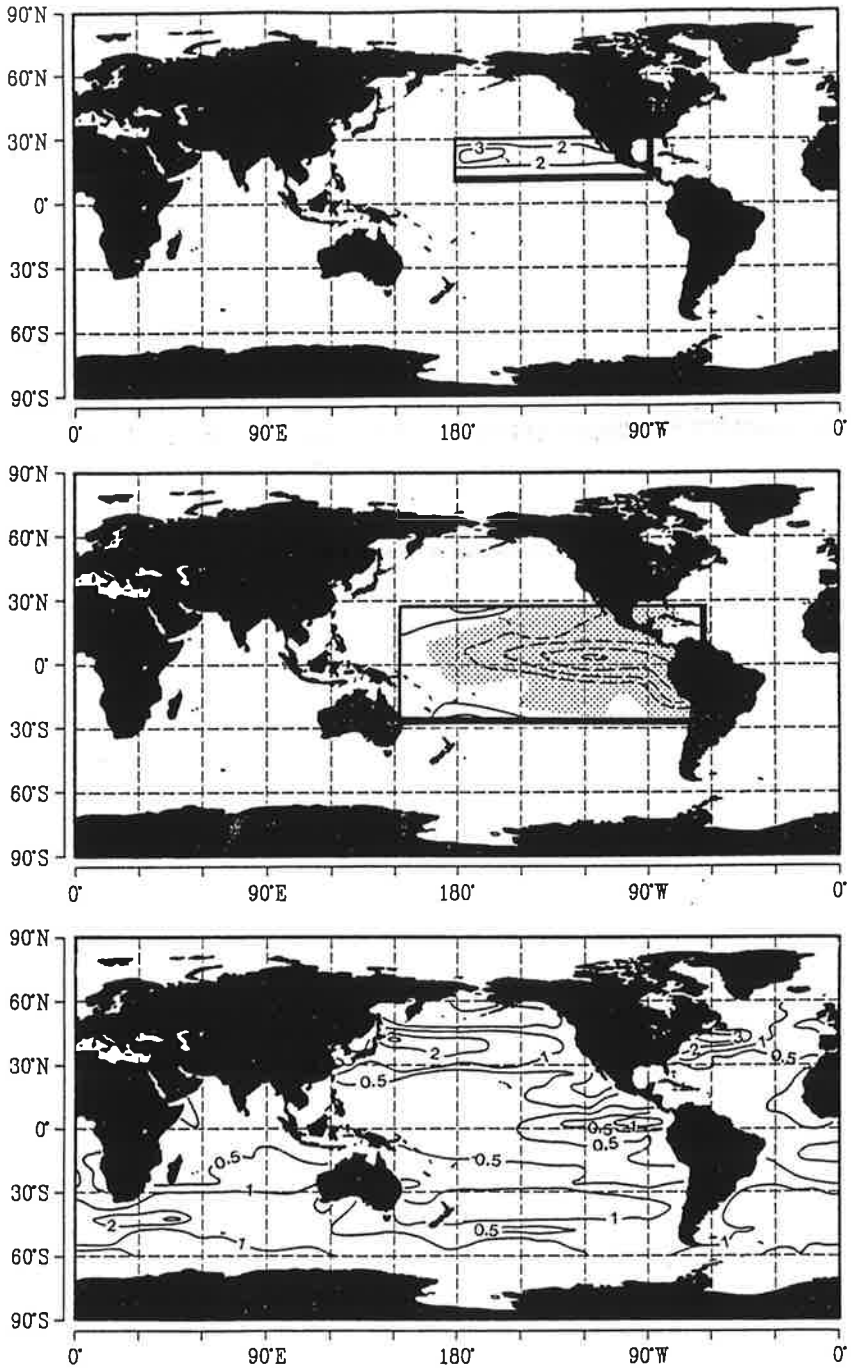

Figure 8

Sea surface temperatures used in the three sensitivity experiments. Isolines: ± 0.5, 1, 2, 3 K.

a) The modification of the anomaly field (Fig. 1) used in the sensitivity experiment on the effect of an warm water pool in the northern subtropics.

b) Anomaly field limited to the tropical Pacific.

c) The $2^{\circ}\times2^{\circ}$spatial standard deviation within each $5.6^{\circ}\times5.6^{\circ}$ box of the T21 Gaussian grid, which is added to the basic SST anomaly (Fig. 1) in the "envelope"-experiment.

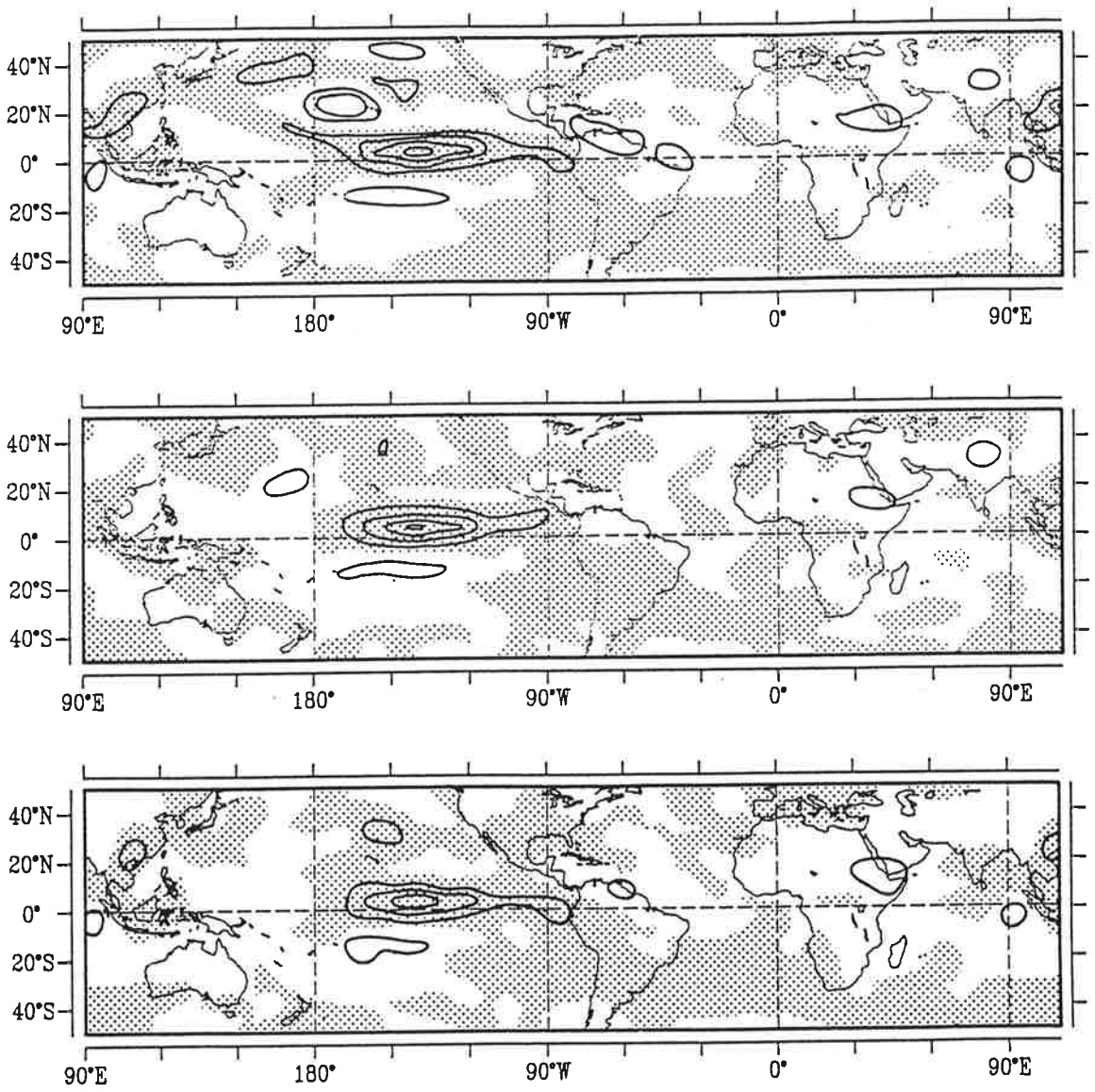

Figure 9

Experiment minus control OLR fields in the three sensitivity experiments. Positive values, indicating reduced convection and rainfall, are stippled. Spacing: 15 Wm^{-2}.

a) Experiment with extra pool of warm water in the northern subtropics of the East Pacific (Fig. 8a).

b) Experiment with SST anomalies limited to the tropical Pacific (Fig. 8b).

c) Experiment with "envelope"-SST anomaly (Fig. 8c)

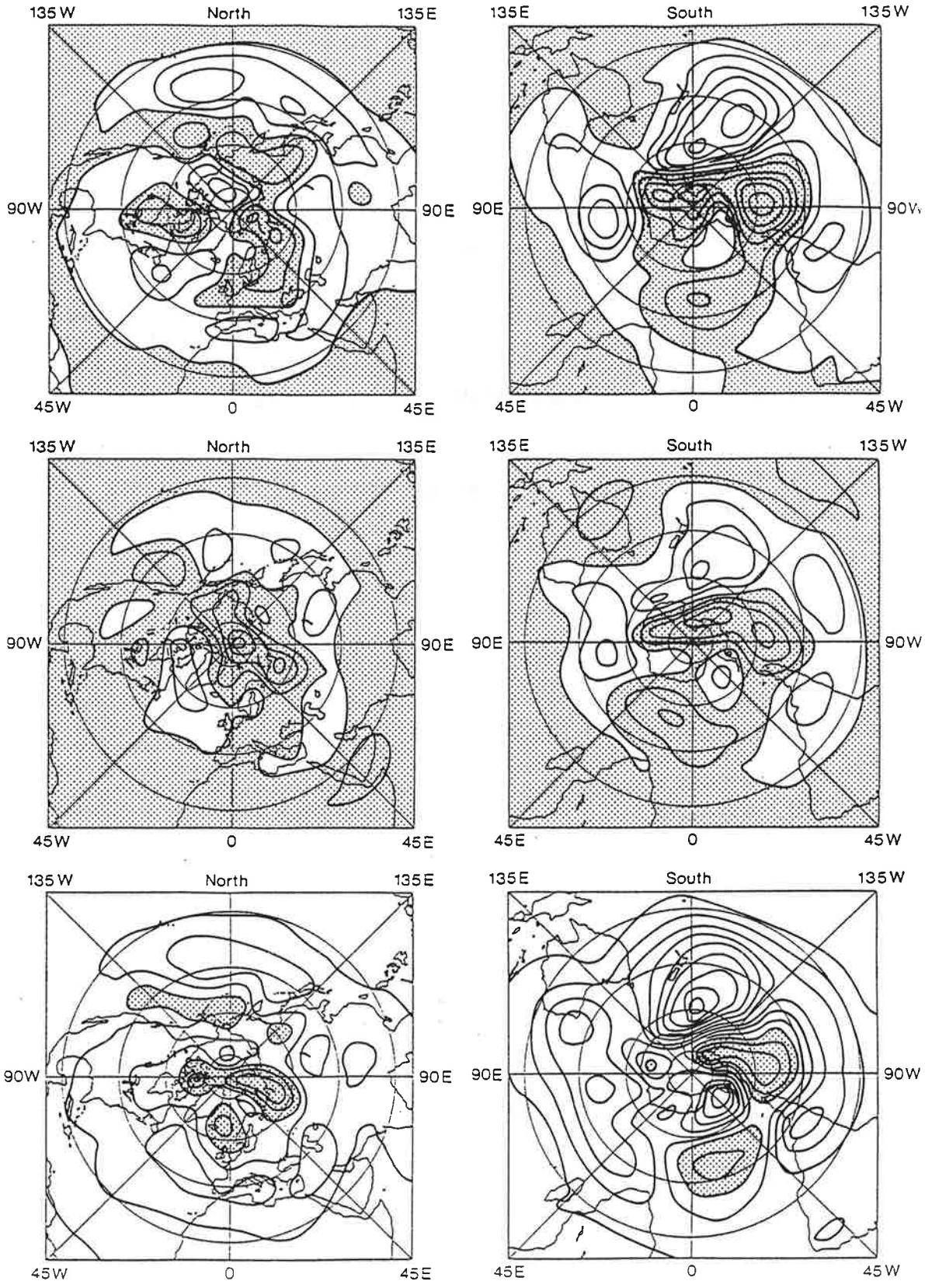

Figure 10

Experiment minus control 500 hPa height fields in the three sensitivity experiments. Spacing: 10 m.

a) Experiment with extra pool of warm water north of the equator in the northern subtropics of the East Pacific (Fig. 8a).

b) Experiment with SST anomalies limited to the tropical Pacific (Fig. 8b).

c) Experiment with "envelope"-SST anomaly (Fig. 8c)

anomalies.

4.2 SST anomalies limited to the Tropical Pacific

To find out the relative importance of the SST anomalies in the Tropical Pacific and of the SST anomalies elsewhere, a sensitivity experiment was done with the SST anomalies limited to the Tropical Pacific. We will see that the response of the basic experiment is similar to this experiment.

The SST anomaly limited to the Tropical Pacific is shown in Fig. 8b and the resulting anomalies of OLR and 500 hPa height in Figs. 9b and 10b, respectively. The OLR anomalies are almost unchanged compared to the basic experiment (Fig. 6b) with OLR enhanced by as much as 60 Wm^{-2} in the East Equatorial Pacific and minor negative anomalies over the West Pacific, the Tropical Atlantic and Africa. The 500 hPa height anomaly field are very similar to the anomalies in the basic experiment. This is especially so in the North Pacific, over the Arctic, and over most of the Southern Hemisphere.

We conclude from this experiment that the performance of the basic experiment (Section 3) is indeed almost entirely controlled by the SST anomalies in the Tropical Pacific.

4.3 The envelope SST formulation

Conventionally, SSTs and SST anomalies in GCM experiments are specified as mean values that are averaged over one grid box. If these grid boxes are large, as is the case in climate models, then the averaging significantly smooths the SST field. The projection of the June 1988 $2^{\circ}\times2^{\circ}$ SST analysis on the $5.6^{\circ} \times 5.6^{\circ}$ Gaussian grid (Fig. 1) of our (T21) GCM masks a substantial amount of sub-grid scale variability. This is demonstrated by the standard deviation of the $2^{\circ}\times2^{\circ}$ SST within each $5.6^{\circ}\times5.6^{\circ}$ grid box (Fig. 7c). Maximum values of 4.5 K and 3.3 K mark the Gulf stream and the Kuroshio, whereas values between 0.2 K and 0.4 K prevail in the tropics except for the cold water tongue in the east equatorial Pacific where values as large as 1 K occur. Typical values in the Southern Ocean are 1 K to 1.5 K. We speculate that sub-grid scale maxima of SST may trigger convection in the tropics. We test an "envelope"-strategy to parameterize the effect of the sub grid scale maxima. In this strategy the tropical SST is increased by the spatial standard

deviation of the full SST field within a grid box. This "envelope"-approach was proposed by Wallace et al. (1983) to parameterize sub grid scale orography.

Conceptually it would be better if this experiment could be compared against a control experiment with an "envelope"-SST distribution in which the effect of the sub-grid scale spatial variability of the time-mean field is taken into account. Unfortunately, the 1979 - 1988 mean field on a $2^{o}\times2^{o}$ grid was not at our disposal at the time of the experiments. Therefore we compare this experiment against our standard control run even if the comparison is not really fair. The OLR signal (Fig. 9c) in the East Pacific is reduced by 25% to 45 Wm^{-2}. This was to be expected as the negative anomalies in the basic experiment are weakened in the East Pacific by 0.5 to 1 K. Otherwise the OLR is only weakly affected by the general increase of SST in the tropics. The 500 hPa height (Fig. 10c) is increased everywhere compared to the basic experiment - which is plausible since the addition of the sub-grid spatial standard deviation increases the overall tropical SST. Besides this general increase, however, the response patterns are again similar to the basic experiment.

5. CONCLUSION AND DISCUSSION

5.1 Summary

Studies of the influence of sea surface temperature anomalies on the extratropical circulation have mainly been concerned with Northern Hemisphere winter conditions. Having been influenced by Karoly's (1989) finding that ENSO SST anomalies appear to stimulate strong Southern Hemisphere flow anomalies during northern summer and Trenberth et al.'s (1988) suggestion that tropical and subtropical heating anomalies contributed to an anomalous flow pattern over North America in June, 1988, we performed GCM experiments concerned with the effects of SST anomalies during northern summer. Focusing on June, 1988 when a large anomalous cold pool existed, the model produced extratropical responses in both hemispheres. Elements of the response were insensitive to details of the experimental design, and SST anomalies equatorward of 30 were primarily responsible for these robust components of the response. In the Northern Hemisphere the recurring response was composed of a three-lobed wavetrain emanating from the equatorial Pacific and terminating on the west coast of North America. Consistent with Webster's (1982) arguments, the Southern Hemisphere (winter) response was stronger than the Northern Hemisphere response, and was comprised of a wavetrain arching from the equatorial Pacific across the Southeast Pacific and South America.

Though our experiments indicate that the sea surface temperature distribution of June, 1988 is capable of producing a distinct, reproducible, extratropical response in our GCM during northern summer, they are probably not very helpful in determining the causes of the prominent extratropical circulation anomalies that actually occurred during June, 1988. Over North America none of the GCM experiments produces the distinctive high which led to drought in late spring and early summer of that year. This failure may be the result of a poor model climate or an incorrect distribution of subtropical eastern Pacific heating anomalies, as the work of Trenberth et al. (1988) and Trenberth and Branstator (1992) would suggest. Indeed, the position of the model Northern Hemisphere wavetrain to the west of the observed wavetrain could be indicative of mispositioned heating anomalies. It may also be that the circulation over North America during June, 1988 was affected by the state of the atmosphere at the beginning of that month, as Mo et al. (1991) have argued, in which case no simulation experiment would be able to capture the observed flow anomalies. In the Southern Hemisphere the simulation seems to have more success in reproducing some of the important observed circulation anomalies, in

particular a wavetrain over the South Pacific and South America. However, in this case, too, it may be misleading to conclude that the GCM is indicating what processes were important in determining the June, 1988 circulation. In the experiments the prominent wavetrain over the South Pacific almost certainly has its origin in the tropical cold pool since it can be traced back to a dipole that straddles the equator (Fig. 5b). This dipole is probably the signature of a negative heating anomaly on the equator, as shown by Gill (1980). On the other hand, in nature the corresponding wavetrain appears to begin in the subtropics; no equatorial dipole is present (Fig. 5c). This suggests different origins for the observed and modeled South Pacific wavetrains.

5.2 Linear Analysis

To try to clarify what may be the sources of the South Pacific wavetrains, we make use of a linear primitive equation model. This is the same multilevel model used by Trenberth and Branstator (1992) in their investigation of Northern Hemisphere heating anomalies during 1988 except the basic state is zonally symmetric and is based on the mean ECMWF analysis for June between the years 1979 and 1989.

First we consider the direct effect of the most prominent SST feature in Fig. 1, the cold equatorial Pacific anomaly. From the positive OLR anomaly in the tropical Pacific in Fig. 6a, we assume the heating anomaly that resulted from this cold patch can be approximated by an elliptically shaped negative heating anomaly that is centered at 5^{o}N, 160^{O}W and has a major axis of 100^{O}, a minor axis of 10^{o}, a $\cos(\pi\sigma)$ vertical structure (where σ is the model's vertical coordinate), and a maximum heating rate of -4K/day. The steady response of the linear model to this idealized source, as represented by streamfunction at σ = .300, is shown in Fig. 11a. Rather like the standard GCM experiment in Fig. 5b, the model response consists of an equatorial dipole and a Southern Hemisphere wavetrain. As we have noted, these features can be understood in terms of Gill's (1980) and Webster's (1982) investigations. This solution qualitatively captures the main features of the GCM Western Hemisphere solutions (except for the second and third lobes of the North American wavetrain which, as shown in Trenberth and Branstator (1992), appear if a zonally asymmetric background is used and are enhanced by heating in the subtropical North Pacific), but clearly it has marked discrepancies as a surrogate for the observed situation (Fig. 5c).

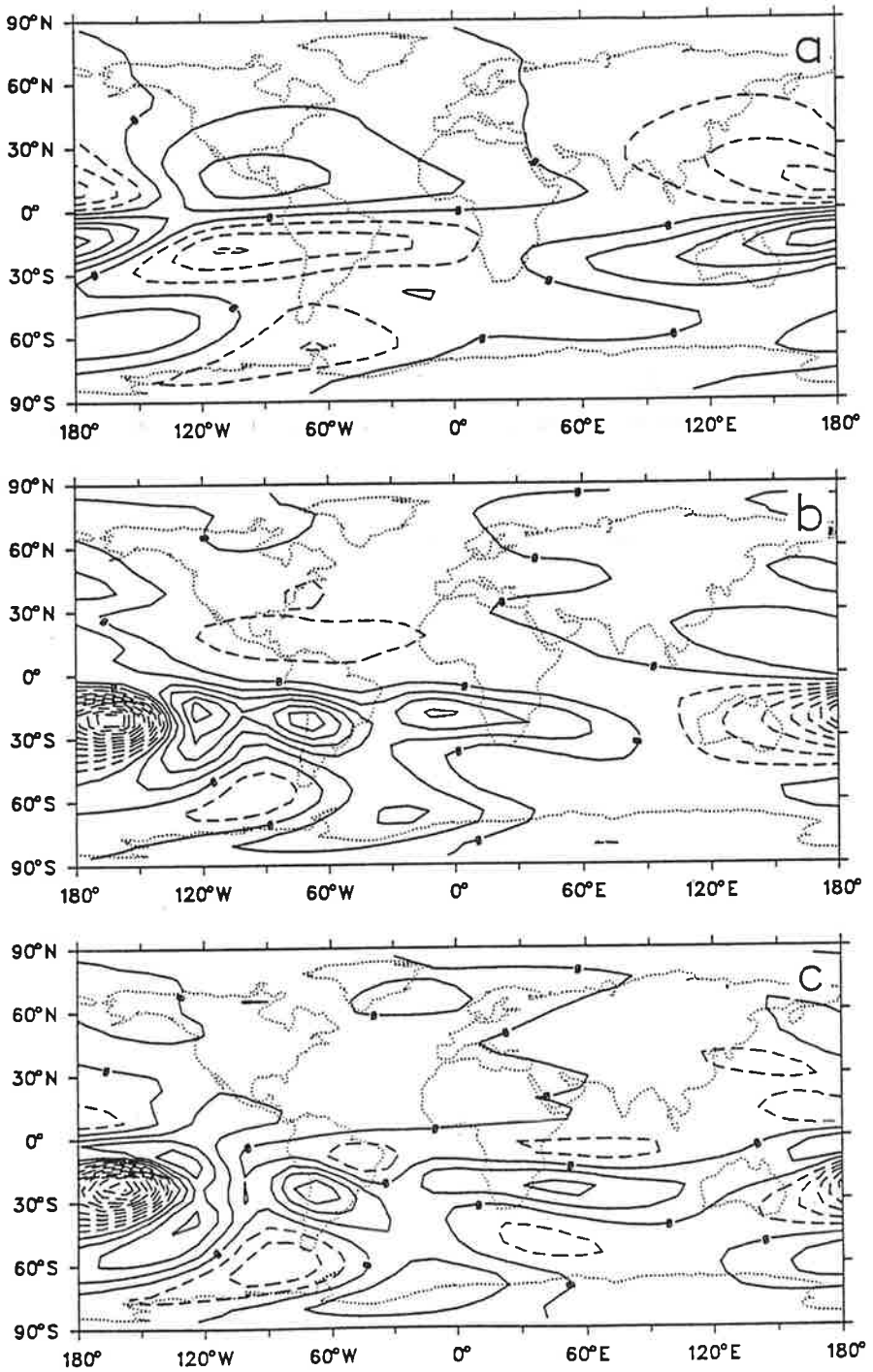

Figure 11

Streamfunction anomaly at σ =.300 in a steady linear model forced by elliptically shaped

a) negative heating center at 5^{o}N, 160^{O}W,

b) positive heating center at 15^{O}S, 160^{O}W, and

c) both sources of a) and b).

Contour interval is $10^{6}m^{2}s^{-2}$.

According to the OLR anomalies of Fig. 6a, the negative equatorial heating anomaly was not the only potentially important source for the Southern Hemisphere during June, 1988. On the dateline of the subtropics was an equally prominent positive heating anomaly. Representing this anomaly by an ellipse centered at 15°S, 160°W and with a 60^0 major axis, 20^o minor axis, and a maximum heating rate of +4K/day, the steady linear response to such a subtropical anomaly is shown in Fig. 11b. This solution indicates that such an anomaly would produce a wavetrain response without the equator-straddling dipole seen in the previous linear solution. The response to this forcing is of higher amplitude than the response to the equatorial forcing because the local divergence field produced by the forcing is a much stronger dynamical source of vorticity given the larger magnitude of planetary vorticity in the subtropics than near the equator. Furthermore, the linear response to the sum of the equatorial and subtropical sources (Fig. 11c) indicates that such a combination could produce a significant Southern Hemisphere response that has only a weak equatorial component, as was observed in June, 1988. From these results we conclude that though our GCM simulations produce a wavetrain in the correct quadrant of the Southern Hemisphere, in effect they have probably omitted a major factor in the formation of the June, 1988 wavetrain. Because the local heating that resulted from equatorial sources was much more dominant in the simulation than it was in nature, the influence of the subtropical heat source was essentially unfelt.

5.3 Discussion: The resolution problem

This hypothesis that our GCM experiments overemphasized the role of the equatorial heating is supported by two 10-year model simulations made with the T42 version of the ECHAM 3 GCM (a slightly improved version of the ECHAM 2 model which we have used in the experiments discussed so far). Each of these two runs was forced with observed SST from 1979 to 1988 so that "June 1988" anomalies (relative to the 1979-1988 ensemble mean) are embedded in each experiment. The two experiments were begun from different initial conditions, so that the two modeled June 1988 circulations are statistically independent.

In Figure 12 the mean June-88 monthly anomalies of OLR and of 500 hPa height from the two high resolution experiments are shown. The two tropical Pacific OLR anomalies have less disproportionate strengths in the two T42 experiments (Fig. 12a) than in the T21 model experiments are (Fig. 6b). Consistent with our previous arguments, the 500 hPa height field anomalies in the Southern

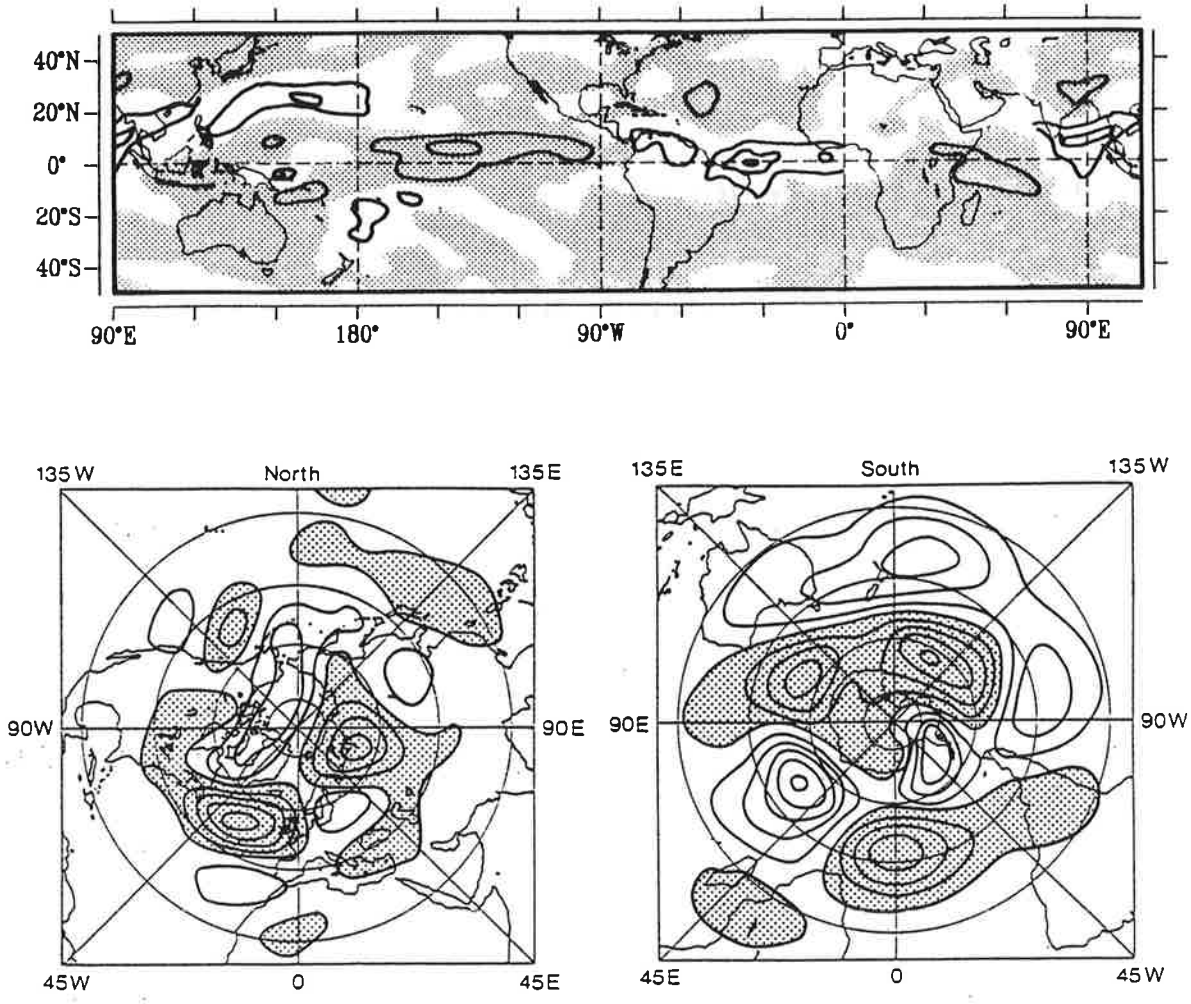

Figure 12

Mean of anomalous fields in June 1988 as simulated in two T42 model runs. The anomalies are calculated relative to the 1979-88 mean.

a) OLR, Contours: ±15 and ±30 Wm^{-2}. Positive values, indicating reduced convection and rainfall, are stippled.

b) Northern Hemisphere 500 hPa height. Spacing: 20 m.

c) Southern Hemisphere 500 hPa height. Spacing: 20 m.

Hemisphere (Fig. 12c) are more realistic (Fig. 7c) than in the T21 model output (Fig. 7d). Also the magnitude of the T42 model response is markedly larger than in the T21 model response. However, the improvement in the horizontal resolution and the simulation of the annual cycle in the T42 experiments does not yield an anomalous circulation in the Northern Hemisphere similar to the state observed in June 1988 (Figs. 12b and 7a).

To summarize our GCM experiments are useful indicators of the likely impact that negative equatorial heating anomalies in the Pacific would have on the extratropics if they acted in isolation, but the experiments are not representing the June, 1988 situation well because they have not done a good job of capturing the global distribution of heating anomalies that occurred in June 1988.

APPENDIX: t-Test and the level of recurrence

Two random variables **X** and **Y** are called *p*-recurrent (von Storch and Zwiers, 1988) if for any realization Y of **Y**: $\mathbf{P}(Y > \mu_X) = p$. Here $\mathbf{P}$ is the probability that the statement in parenthesis is correct and μ_X is the mean of X. If **X** and **Y** are both normally distributed and share the same variance σ^2 then *p*-recurrence is equivalent to

$$\tilde{t} = \frac{\mu_Y - \mu_X}{\sigma^2} \geq Z_p$$

Here Z_p is the *p*-quantile of the standard normal distribution. If the true parameters μ_X, μ_Y and σ^2 are replaced by the respective estimated numbers the number $\tilde{t}\cdot(n/2)^{1/2}$ is t-distributed with 2(n-1) degrees of freedom if n independent samples of **X** and and n independent samples of **Y** are available and if the null hypothesis $\mu_X = \mu_Y$ is valid. Thus *p*-recurrence is sufficient evidence to reject the null hypothesis with a risk of α, given that the critical value $t_{\alpha,2(n-1)} = \tilde{t}\cdot(n/2)^{1/2}$. If n is increased, a smaller level of recurrence is required for a rejection at a fixed risk α.

We had in our experiment 22 consecutive months so that we have approximately n = 16 independent realizations in the SST-experiment and in the control run. With this n a p = 80% level of recurrence goes with a risk of rejecting the two-sided null hypothesis $\alpha \approx 3.6\%$ and an α = 1% goes with $p \approx 85\%$.

ACKNOWLEDGEMENTS

We are thankful to Dick Reynolds for supplying us with the SST data, to Heiko Borgert and Ulrich Schlese who helped us to set up the experiments. Thomas Sperling and Ute Luksch helped us with the ECMWF analyses, the use of which was permitted by the Deutscher Wetterdienst. Ortrun Roll prepared the latitude-height sections. Doris Lewandowski and Marion Grunert prepared the diagrams. This study was in part financed by the European Community through the project EPOCH 0003-C "Climate of the 21st Century" and Bundesministerium für Forschung und Technologie project 07KFT30.

REFERENCES

Blackmon, M.L.; J.E. Geisler, and E.J. Pitcher, 1983: A general circulation model study of January climate anomaly patterns associated with interannual variations of equatorial Pacific sea surface temperatures. - J. Atmos. Sci. 40, 1410-1425

Cubasch, U., 1985: The mean response of the ECMWF global model to the El Niño anomaly in extended range prediction experiments. - Atmosphere-Ocean 23, 43-66

Cubasch, U., K. Hasselmann, H. Höck, E. Maier-Reimer, U. Mikolajewicz, B.D. Santer and R. Sausen, 1992: Time-dependent greenhouse warming computations with a coupled ocean-atmosphere model. - Clim. Dyn. 8, 55-69

Deutscher Wetterdienst, 1988: Monthly Global Climate Review 36, No. 6. (Bernhard Nocht Str. 76, 2000 Hamburg 4, Germany)

Folland, C.K. and D.E. Parker, 1990: Observed variations of sea surface temperature. - M.E. Schlesinger (ed.): Climate-Ocean Interaction, 21-52

Gill, A., 1980: Some simple solutions for heat-induced tropical circulation. - Quart. J. Roy. Met. Soc. 106, 447-462

Karoly, D., 1989: Southern hemisphere circulation features associated with El Niño - Southern Oscillation events. - J. Climate 2, 1239-1252

Lau, K.M. and L. Peng, 1992: Dynamics of atmospheric teleconnections during northern summer. - J. Climate 5, 140-172

Mo, K.C., J.R. Zimmerman, E. Kalnay and M. Kanamitsu, 1991: A GCM study of the 1988 United States drought. - Mon. Wea. Rev. 119, 1512-1532

Mo, K.C. and E. Kalnay, 1991: Impact of sea surface temperature anomalies on the skill of monthly forecasts. - Mon. Wea. Rev. 119, 2711-2793

Palmer, T.N. and C. Brankovic, 1989: The 1988 U.S. drought linked to anomalous sea-surface temperature. - Nature 338, 554-557

Roeckner, E., L. Dümenil, E. Kirk, F. Lunkeit, M. Ponater, B. Rockel, R. Sausen, U. Schlese, 1989: The Hamburg version of the ECMWF model (ECHAM) GARP

Report 13, WMO Geneva WMO/TP 332

Ropelewski, C.F., 1988: The global climate for June-August 1988: A swing to the positive phase of the Southern Oscillation, drought in the United States and abundant rain in the monsoon areas. - J. Climate 1, 1153-1174.

Trenberth, K., G.W. Branstator and P. A. Arkin, 1988: Origins of the 1988 North American Drought. - Science 242, 1640-1645

Trenberth, K.E. and G.W. Branstator, 1992: Issues in establishing causes of the 1988 drought over North America. - J. Climate 5, 159-172

Ulbrich, U., G. Bürger, D. Schriever, H. von Storch, S.L. Weber and G. Schmitz, 1993: The effect of a regional increase in ocean surface roughness on the tropospheric circulation: A GCM experiment. - Clim. Dyn. 9 (in press)

U.S. Department of Commerce, 1988: Climate Diagnostics Bulletin June 1988 - near real-time analyses ocean/atmosphere, 88/6. - Climate Analysis Center, Washington D.C.

von Storch, H., and F.W. Zwiers, 1988: Recurrence analysis of climate sensitivity experiments. - J. Climate 1, 157-171

Wallace, J.M., S. Tibaldi and A.J. Simmons, 1983: Reduction of systematic errors in the ECMWF model through the introduction of an envelope orography. - Quart. J. Roy. Met. Soc. 109, 683 - 717

Weber, S., H. von Storch, P. Viterbo, L. Zambresky, 1993: Coupling an ocean wave model to an atmospheric general circulation model. - Clim. Dyn. 9 (in press)

Webster, P., 1982: Seasonality in the local and remote atmospheric response to sea surface temperature anomalies. - J. Atmos. Sci. 39, 41-52

Wright, P.B., 1984: Relationships between indices of the Southern Oscillation. - Mon. Wea. Rev. 112, 1913-1919

Wright, P.B., 1989: Homogenized long-period Southern Oscillation indices. - Intl. J. Climatol. 9, 33-54